

1 Binding Selectivity Studies of Phosphoinositide 3-Kinases Using Free Energy Calculations

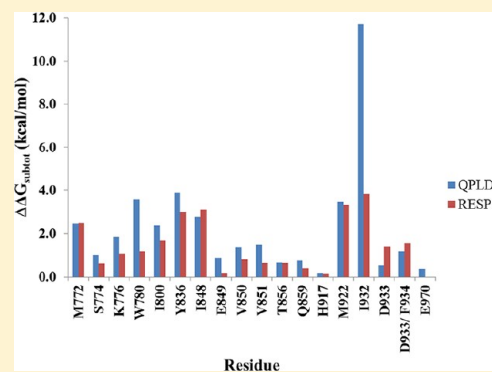
2 Dima A. Sabbah,[†] Jonathan L. Vennerstrom,[†] and Haizhen A. Zhong^{*,‡}

4 [†]College of Pharmacy, University of Nebraska Medical Center, 986025 Nebraska Medical Center, Omaha, Nebraska 68198-6025,
5 United States

6 [‡]DSC 362, Department of Chemistry, The University of Nebraska, 6001 Dodge Street, Omaha, Nebraska 68182, United States

7 **S** Supporting Information

8 **ABSTRACT:** Phosphoinositide 3-kinases (PI3Ks) and their phosphatidylinositol 3,4,5-triphosphate (PIP₃) products regulate a variety of cellular processes. Of these, PI3K α is an attractive target for anticancer drug design. Mutations in the PI3K α kinase domain alter the mobility of the activation loop resulting in gain of function. We employed molecular dynamics (MD) simulations-based energetic analysis using molecular mechanics/generalized born surface area (MM/GBSA) for PI3K α and γ . MD simulations were carried out for PI3K models based on the RESP (restrained electrostatic potential) and quantum mechanics (QM)-polarized ligand docking (QPLD)-derived partial charges. Computational alanine scanning was also used to evaluate the contributions of key binding residues to ligand binding. Our results show that both QPLD and RESP charge models of PI3K α provide similar performance in MD simulations and consequently comparable binding free energies. Binding free energies for both PI3K γ models (−9.5 and −9.3 kcal/mol) and PI3K α models (−10.9 and −11.7 kcal/mol) were in good agreement with experimental values. A significant loss in binding free energy was observed when hydrophobic residues were mutated to alanine, suggesting that specific hydrophobic interactions are important to optimal ligand binding. MM/GBSA calculations suggested that residues Ser774, Gln859, and Ile932 of PI3K α might be used to design H1047R mutant-specific ligands, whereas Lys890 of PI3K γ can be used for ligand design targeting PI3K γ .



1. INTRODUCTION

26 Phosphatidylinositol 3-kinases (PI3Ks) phosphorylate phosphatidylinositol 4,5-bisphosphate (PIP₂) to generate phosphatidylinositol 3,4,5-triphosphate (PIP₃), an important second message coordinating the activities of PI3K downstream effectors such as AKT. The activation of PI3K/AKT signaling triggers cell proliferation, growth, angiogenesis, and metastasis. Aberrations in the PI3K/AKT pathway have been observed in a number of human cancers.¹ There are three families of class IA PI3Ks, each with distinct substrate specificity and primary structures, p110 α , p110 β , and p110 δ isoforms, encoded by PIK3CA, PIK3CB, and PIK3CD, respectively. PI3K γ , the only class IB PI3K protein, is a structural homologue of PI3K α . PI3K α and PI3K β are ubiquitous in mammalian tissues, whereas PI3K δ and PI3K γ mainly are present in leukocytes.² PIK3CA, the coding gene of PI3K α , is mutated and amplified in numerous human tumors. PI3K α is the principal isoform regulating tumor growth and proliferation, whereas PI3K γ mediates inflammatory pathways and is considered as a target for rheumatoid arthritis and asthma.³ Numerous inhibitors have been reported to inhibit both PI3K γ and PI3K α ; only a few of these are α -isoform selective. Selective inhibition of PI3K α has been considered as a viable approach for cancer treatment. Thus, to assist future structure-based drug design, we investigated binding site differences between these two PI3K

isoforms to identify residues associated with selective ligand binding. The selection of PI3K α and γ was also based on the availability of crystal structures for these two isoforms.

PIK3CA mutations and amplification have been found in colon, breast, brain, and endometrial cancers.^{4,5} The majority of these mutations are located in the helical (E542K and E545K) and the kinase (H1047R) domains. These “hot-spot” mutations enhance the in vitro kinase activity of PI3K α , a phenomenon described as “gain-of-function.”^{6,7} Using human mammary epithelial cells (HMEC), Liu et al. found that mutations of E545K and H1047R activated the AKT signaling cascade and produced genetic transformations.⁸ Although PIK3CA mutations have been found in more than 30% of colon and breast cancer patients,⁴ only 7.1% of gastric cancer patients carried these same mutations; however 67% of the latter patients had amplifications in PIK3CA,⁹ indicating that inhibition of wild-type PI3K α may be a viable approach to suppress gastric tumor cell growth. In patients with primary colorectal adenocarcinomas (CRC) and associated hepatic metastases, 17 out of 21 were characterized with variance in EGFR mutational status between the primary CRC and liver metastases; in this same patient population, only 4/21 had mutational variability. No

Received: June 29, 2012

72 variants were detected in PIK3CA codons 542, 545, and
73 1047,¹⁰ indicating that inhibition of the H1047R mutant of
74 PI3K α would be effective in patients with both primary tumors
75 and metastases.

76 To guide PI3K inhibitor design, we employed computational
77 methods to investigate the role of individual residues in ligand
78 binding. Han and Zhang carried out molecular dynamic (MD)
79 simulations of the kinase domains of the α and γ isoforms of
80 PI3K and observed that residues Trp780 and Asn782 in PI3K α
81 (Trp812 and Glu814 in PI3K γ , respectively) could confer
82 isoform specificity.¹¹ Our docking studies indicated that
83 structural differences in the kinase loop and residues Gln859,
84 Ser854, Tyr836, and Ser774 of PI3K α could be exploited to
85 design isoform-specific or mutant-active inhibitors.¹²

86 The PI3K α D915A mutant and D933A/F934A double
87 mutant both show a complete loss of kinase activity, whereas
88 the E970A mutant had little effect.¹³ PI3K α gatekeeper mutants
89 I848A, I848G,¹⁴ I848L, I848S, and I848 V¹⁵ showed losses in
90 catalytic activities, whereas mutant H1047R enhanced the lipid
91 kinase activity (relative to the wild-type).^{6,16} Additional
92 mutations in the H1047R strain led to three different
93 outcomes: unchanged, potentiated, or weakened kinase
94 activities. For example, the C838A, C838T, and G837 M
95 double mutants retained the same activities as H1047R; the
96 S854A and G837N mutants potentiated the kinase activities of
97 H1047R, and the L814C, L814N, I800L, I800M, and I848 V
98 mutants weakened or abolished the activity of H1047R. Various
99 PI3K inhibitors have a range of potencies against these double
100 mutants: the PI3K inhibitors PIK-90, PIK-93, PI-103, PP-110,
101 PW-12, and BEZ-235 are less potent against the I848 V and
102 I800 M mutants, whereas PIK-90, PIK-93, and PP-110 are
103 more potent against the H1047R mutant.¹⁵ The potentiating or
104 weakening effects of these binding residue mutations, however,
105 were observed only for the H1047R mutant, and not for the
106 wild-type PI3K α .

107 To design isoform- or mutant-selective inhibitors, it is
108 necessary to understand the effects of residue mutations in the
109 enzyme active site. In this work, we systematically investigated
110 how active site mutations affected ligand binding for the wild-
111 type (WT) and H1047R mutant (MUT) PI3K α , and PI3K γ .
112 We employed molecular dynamic (MD) simulations-based
113 molecular mechanics/generalized Born surface area (MM/
114 GBSA) calculations and computational alanine scanning.^{17,18}
115 To investigate the effect of charge models on ligand binding in
116 our MD simulations, we applied conventional RESP (restrained
117 electrostatic potential) charges and quantum mechanics (QM)-
118 polarized ligand docking (QPLD)-derived partial charges for
119 bound ligands. QPLD-derived partial charge models have
120 shown improvements in predicting docking conformations¹⁹
121 and for estimating the binding free energies of DNA/ligand
122 interactions.²⁰ However, no protein–ligand interactions based
123 on the QPLD-based charge model have been reported. To our
124 best knowledge, this is the first QPLD-based MM/GBSA
125 calculation for kinase/ligand interactions.

2. COMPUTATIONAL METHODS

126 **2.1. Preparation of Isoforms.** The X-ray crystal structures
127 of apo PI3K α (PDB ID 2RD0),¹⁶ the mutant (H1047R)
128 PI3K α /wortmannin complex (PDB ID 3HHM),⁶ and the
129 PI3K γ /LY294002 complex (PDB ID 1E7 V)²¹ were retrieved
130 from the RSCB Protein Data Bank. The wortmannin
131 coordinates of 3HHM were adopted to 2RD0 and used as a

ligand. Four missing sequences in 2RD0 and 3HHM were fixed
as described¹² using the homology module in MOE.²²

2.2. Restrained Electrostatic Potential (RESP) Charge.
The RESP partial charges for wortmannin were developed as
follows. First wortmannin was optimized using HF/6-31G* ab
initio calculations with Gaussian 03.²³ Then, the RESP charges
were derived using the ANTECHAMBER script in
AMBER10.²⁴ The atom types and the stretching, bending,
dihedral, and improper dihedral parameters for both
wortmannin and LY294002 were assigned based on the
Generalized AMBER Force Field (GAFF).²⁴ The atom types
and the atomic partial charges of these two ligands are listed in
Supporting Information Tables 1S and 2S.

2.3. Quantum Mechanics Polarized Ligand Docking (QPLD)-Based Charges. In contrast to the RESP charges of a
ligand calculated in a vacuum, QPLD-based partial charges are
calculated in the environment of a protein structure. QPLD
charges were developed using the QPLD protocol in the
Schrödinger software suite.²⁵ Wortmannin was docked to
PI3K α wt, PI3K α H1047R mutant, or PI3K γ , and the resulting
protein/ligand complexes were optimized with wortmannin
treated by the QM approach and the protein treated by the
molecular mechanics (MM) method using the QSite program.
The QM/MM procedure determines a new set of atomic
partial charges for the ligand based on QM calculations and
takes into account the protein that was minimized with the MM
force field. The minimized ligands (in the protein environ-
ment) were redocked to the protein active site and the docked
pose with the lowest root-mean-square deviation (RMSD) from
the reference was adopted and its partial charges were used for
MD simulations.

2.4. Molecular Dynamics (MD) Simulations. Established
procedures^{12,18} for MD simulations were carried out using the
AMBER 10 package²⁴ with the AMBER 99SB force field.²⁶
Briefly, residues Asp and Glu were assigned to -1 charges, and
Lys and Arg were assigned $+1$ charges. The orientation of Asn,
Gln, and His side chains were optimized to maximize H-bond
interactions using the Protein Preparation Wizard in
Schrödinger.²⁵ Each system was neutralized with sodium ions
and soaked in a rectangular box of TIP3P water molecules²⁷
extended 10 Å away from any protein atom: 6 Na⁺ and 1151
water molecules were added to 1E7 V (box size 68 × 69 × 80 Å
for both RESP and QPLD charge models); 1 Na⁺ and 5562
water molecules were added to 3HHM (box size 84 × 83 × 94
Å for both RESP and QPLD charge models); and 2 Na⁺ and
6277 water molecules were added to 2RD0 (box size 83 × 83 ×
98 Å for both RESP and QPLD charge models). Each system
was subjected to a 1000 step minimization using the steepest
descent algorithm to reduce the steric clashes, followed by a
heating process for 30 ps from 10 to 300 K, and an
equilibration for 100 ps at 300 K. The production simulations
were carried out using the NPT ensemble with a time step of 1
fs and 4000 snapshots were collected during 4000 ps. For the
3HHM RESP model, a 12 ns simulation was carried out and
the last 4 ns snapshots were used to obtain free energy and
RMSD data. The 10 Å nonbonded cutoff was set to define the
van der Waals interaction, and the particle mesh Ewald (PME)
method was used to describe long-range electrostatic
interactions.²⁸ All bonds involving hydrogen atoms were
constrained using the SHAKE algorithm. Constant temperature
and pressure (300 K/1 atm) were maintained by using
Langevin dynamics to regulate temperature with a pressure
relaxation time of 1 ps.

195 After MD simulations, the RMSDs of the backbone atoms
196 for six model systems (3 proteins in two charge models) were
197 obtained using the PTRAJ module in the AMBER 10 package
198 to monitor stability of the protein systems.

199 **2.5. Free Energy Calculations and Computational**
200 **Alanine Scanning.** The GBSA (molecular mechanics/
201 Generalized Born surface area) method was used to calculate
202 the free energy of binding (ΔG_{bind}).^{29,30} The free binding
203 energy can be estimated using eq 1

$$\Delta G_{\text{binding}} = \Delta G_{\text{water}}(\text{complex}) - [\Delta G_{\text{water}}(\text{protein}) + \Delta G_{\text{water}}(\text{ligand})] \quad (1)$$

204 where $\langle G_{\text{water}} \rangle$ is the average free energy of the system
205 calculated by eq 2

$$\langle G_{\text{water}} \rangle = \langle E_{\text{bond}} \rangle + \langle E_{\text{angle}} \rangle + \langle E_{\text{torsion}} \rangle + \langle E_{\text{electrostatic}} \rangle + \langle E_{\text{vdw}} \rangle + \langle G_{\text{GB}} \rangle + \langle G_{\text{SA}} \rangle - \text{TS} \quad (2)$$

208 The broken brackets, $\langle \rangle$, indicate that the free energy and the
209 individual energetic components are average values of all
210 snapshots collected over the 4 ns simulation period. Bond,
211 angle, torsion, electrostatic, and vdw energy terms were
212 calculated based on gas phase geometries. Solvation free
213 energies were calculated based on polar (G_{GB}) and nonpolar
214 (G_{SA}) energies. The polar term was evaluated using the
215 Generalized Born theory (GB program in AMBER package)³¹
216 and the nonpolar contributions due to solvation were estimated
217 with the program MSMS.³² The average entropy, S , was
218 estimated using NMODE module^{33,34} based on 10 snapshot
219 configurations. All energy components and solvation contribu-
220 tions were calculated using 4 ns MD extracted trajectories for
221 the ligand/protein complexes.

222 To investigate the impact of mutational effects on ligand
223 binding, each residue within the 4.5 Å of the bound ligands was
224 computationally mutated to alanine using the MM/GBSA
225 method. The free energy changes ($\Delta\Delta G_{\text{bind}}$) were defined as
226 $\Delta G_{\text{bind}}(\text{mutant}) - \Delta G_{\text{bind}}(\text{wild-type})$ for a potential mutation
227 from wt to mut. A positive $\Delta\Delta G_{\text{bind}}$ indicates that ligand
228 binding to the wild-type protein is more favorable (i.e., less
229 favorable to the mutant), as $\Delta G_{\text{bind}}(\text{wild-type})$ is more
230 negative. On the other hand, a mutation resulting in a more
231 negative $\Delta\Delta G_{\text{bind}}$ is considered to be more favorable.

3. RESULTS AND DISCUSSION

232 **3.1. Molecular Dynamics (MD) Simulations.** The root-
233 mean square deviations (RMSDs) of all three proteins (WT
234 PI3K α , 2RD0; MUT H1047R PI3K α , 3HHM; and PI3K γ /
235 LY294002 complex, 1E7V) under two charge models were
236 calculated as a function of time after a backbone least-squares
237 fit. Supporting Information Figure 1S shows that stable RMSD
238 profiles were observed in all simulations: the last 4 ns of the
239 3HHM (RESP) and other PI3K α models (2RD0 in both
240 charge models and 3HHM in QPLD model) showed similar
241 stabilities. In reference to the starting crystal structure backbone
242 atoms, the average RMSDs of all six models showed that for
243 wortmannin binding to WT PI3K α , the QPLD charge model
244 offers trajectories with less deviation to the starting structure,
245 whereas for the RESP charge model, the RMSDs are smaller in
246 the H1047R mutant and the PI3K γ models. The standard
247 deviations of the PI3K α H1047R MUT and the PI3K γ models
248 were lower than those derived from the QPLD charge model,
249 whereas the QPLD charge model generates a slightly smaller

standard deviation than that of the wild-type PI3K α model
(Table 1). Therefore, although the QPLD-based charge model 251 11

Table 1. Average and Standard Deviations (SD) of RMSDs of MD-Generated Trajectories for All Three Proteins in Two Different Charge Models (2RD0 for wt-PI3K α /wortmannin, 3HHM for H1047R mutant PI3K α /wortmannin, and 1E7V for PI3K γ /LY294002)

	RESP charge models			QPLD charge models		
	2RD0	3HHM	1E7V	2RD0	3HHM	1E7V
mean	2.4	2.0	1.7	2.1	2.7	2.0
SD	0.3	0.5	0.2	0.2	0.3	0.3

has found great success in ligand docking¹⁹ and DNA/ligand
interactions,²⁰ it does not offer a noticeable improvement over
the RESP charge model in terms of the RMSDs of trajectories
of these protein/ligand interactions, presumably because of
hydrophobic binding pockets in kinases.

3.2. Free Energy Calculations and Model Validation.

To determine which factors are more important for ligand
binding in the six model systems, binding free energies and
individual energy components were determined using the MM/
GBSA method (Table 2). Model validation was accomplished
by comparing our calculated free energy values (ΔG_{bind}) for the
PI3K γ /LY294002 complex (-9.5 , and -9.3 kcal/mol for the
RESP and QPLD models, respectively) to the apparent PI3K γ
 K_d of 210 nM for LY294002, which corresponds to a calculated
 ΔG_{bind} of -9.2 kcal/mol.²¹ This ΔG_{bind} was calculated based on
the formula of $\Delta G_{\text{bind}} = RT \ln(K_d)$.^{35,36} Our free energy
calculations show that both QPLD and RESP charge models
are able to predict the experimentally determined free energy of
binding (ΔG_{bind}) of a protein/ligand complex (1E7V/
LY294002). It is conceivable that the HF/6-31G* level of
theory overestimates the in vacuum calculated electrostatic
potential and thus can de facto effectively polarize solutes. The
effectiveness of applying RESP partial charges to small
molecules has been demonstrated in the influenza A virus
neuraminidase³⁷ and DNA/netropsin³⁸ simulations.

Wortmannin is a first-generation nonselective PI3K inhibitor.
It inhibits both PI3K α and γ with IC₅₀ values of 12 and 4.2 nM,
respectively.²¹ The ΔG_{bind} of wortmannin (-10.9 and -11.7
kcal/mol for the respective RESP and QPLD models) to WT
PI3K α are in good agreement with experimental data
($\Delta G_{\text{bind}}(\text{exp})$ of wortmannin: -10.9 kcal/mol). For the same
charge model, the ΔG_{bind} in the H1047R mutant model is
slightly more negative than that in the WT model, indicating
that wortmannin binds more tightly to the mutant protein. This
is in accord with the fact that H1047R mutant caused a gain-of-
function in the lipid kinase activities and with our previous
docking affinity prediction that wortmannin binds more tightly
to the mutant.^{12,39}

Analyses of the energy components for all six models reveal
that the intermolecular van der Waals force (E_{vdw}) is the biggest
contributor for ligand binding to PI3K (Table 2). Because of
the hydrophobic PI3K binding pocket, this outcome is not
surprising; more than half of the residues within 4.5 Å of
wortmannin or LY294002 are hydrophobic.¹² Both E_{vdw} and
the nonpolar solvation contribution ΔG_{SA} drive the interactions
between PI3Ks (both α and γ isoforms) and their ligands. The
value of ΔG_{SA} is proportional to the solvent accessible surface
areas that are buried during the complexation process. The
favorable effect of burying hydrophobic residues during ligand 300

Table 2. Energy Components and Binding Free Energies for Three Proteins in Two Different Charge Models (2RD0 for WT PI3K α /wortmannin, 3HHM for H1047R MUT PI3K α /wortmannin, and 1E7V for PI3K γ /LY294002)

	RESP charge models			QPLD charge models		
	2RD0 (WT)	3HHM (MUT)	1E7V	2RD0 (WT)	3HHM (MUT)	1E7V
ΔE_{elec}	-19.0 ± 4.7	-28.4 ± 3.8	-6.8 ± 3.0	-20.4 ± 3.6	-35.7 ± 4.4	-21.9 ± 3.1
ΔE_{vdw}	-50.3 ± 2.9	-51.0 ± 2.8	-35.2 ± 2.8	-49.4 ± 2.6	-50.6 ± 2.7	-39.3 ± 1.8
ΔG_{SA}	-5.9 ± 0.3	-6.2 ± 0.2	-4.4 ± 0.3	-5.8 ± 0.2	-6.3 ± 0.2	-5.2 ± 0.2
ΔG_{GB}	39.0 ± 4.6	40.3 ± 3.0	14.9 ± 3.0	32.9 ± 3.2	46.0 ± 4.0	28.7 ± 2.3
ΔG_{solv}	33.0 ± 4.5	34.1 ± 3.0	10.6 ± 2.8	27.1 ± 3.1	39.7 ± 3.9	23.5 ± 2.3
ΔG_{subtot}	-36.3 ± 2.8	-45.3 ± 2.7	-31.4 ± 2.9	-42.7 ± 2.7	-46.6 ± 2.7	-37.6 ± 1.9
$-T\Delta S$	25.4	32.6	21.9	31.0	34.0	28.3
ΔG_{bind}	-10.9	-12.7	-9.5	-11.7	-12.6	-9.3

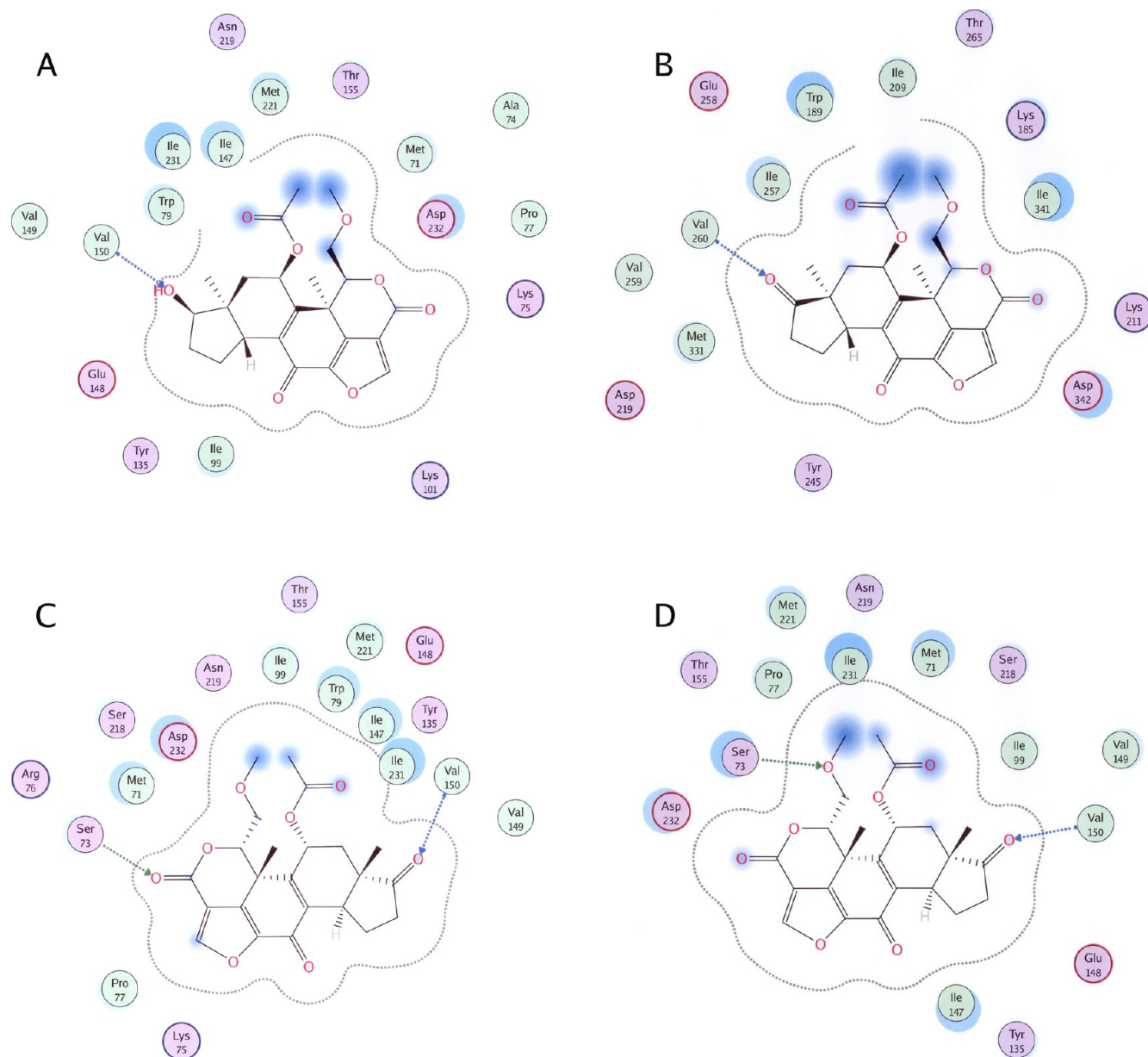


Figure 1. Binding interactions between PI3K/ligand; (A) 2RD0/wortmannin (wt RESP model), (B) 2RD0/wortmannin (wt QPLD model), (C) 3HHM/wortmannin (MUT QPLD model), and (D) 3HHM/wortmannin (MUT RESP model). For A, C, and D, 701 was added to given residue numbers to match residue numbers in PDB; for B, addition of 591 was needed to match residue numbers in PDB. Color codes: red circle, acidic residues; blue circle, basic residues; pink dots, polar residues; green dots, hydrophobic residues; blue dash line, backbone H-bonds; green dash line, side chain H-bonds.

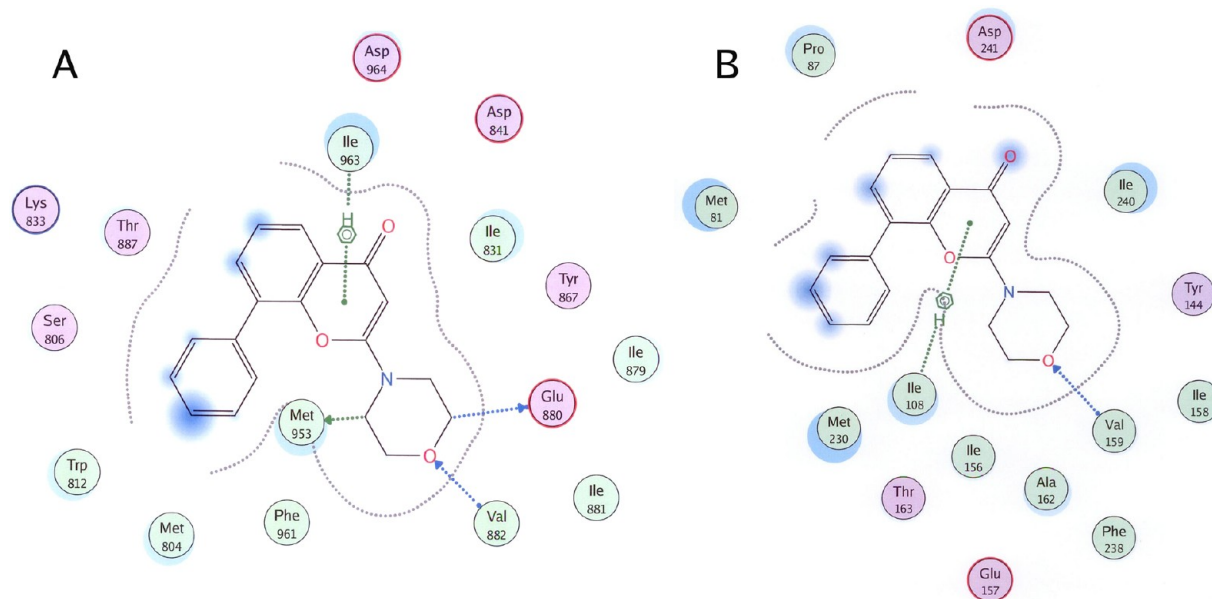


Figure 2. Binding interactions between 1E7V/LY294002: (A) X-ray native structure, (B) QPLD model. Adding 723 to the given residue numbers matched those in the PDB. Color codes: red circle, acidic residues; blue circle, basic residues; pink dots, polar residues; green dots, hydrophobic residues; blue dash line, backbone H-bonds; green dash line, side chain H-bonds.

binding is slightly larger in PI3K α than in PI3K γ . The contributions of ΔE_{vdw} and ΔG_{SA} are comparable in the RESP and the QPLD charge models.

The most noticeable difference between these two charge models and between the α and γ isoforms lies in electrostatic interactions. The RESP charge model appears to underestimate electrostatic contributions for all three protein model systems (PI3K α WT, H1047R MUT, and PI3K γ , Table 2). Charged residues within 4.5 Å of wortmannin in the WT PI3K α binding pocket are Lys776, Lys802, Glu849, and Asp933 (Figure 1A). In the QPLD model, Asp810 was drawn closer to the active site, resulting in a larger electrostatic contribution (Figure 1B). Mutation of His1047 to Arg (3HHM model) in the mutant results in stronger electrostatic interactions (i.e., more negative numbers) and allows the formation of an additional H-bond with Ser774 for ligand binding; thus $\Delta E_{\text{electrostatic}}$ for 3HHM and 2RD0 is -28.4 and -19.0 kcal/mol, respectively. Because of an increase in charge potential in the 3HHM model, it is reasonable to observe a larger electrostatic contribution of -35.7 versus -28.4 kcal/mol in the QPLD vs RESP charge models. In the QPLD model, wortmannin in the H1047R PI3K α complex is surrounded by charged residues Lys776, Arg777, Glu849, and Asp933 (Figure 1C), whereas in the RESP charge model, only Glu849, and Asp933 (Figure 1D) are within 4.5 Å of the ligand. The presence of two positive charged residues (Lys776 and Arg777) increases the positively charged potential, allowing more favorable electrostatic interactions with the partially negatively charged oxygen atoms of wortmannin. Although the individual energy components varied between different charge models, the binding free energies were very similar. This additive characteristic has also been observed in free energy calculations based on the free energy perturbation method.^{40,41}

Electrostatic and VDW contributions are even more significant in the QPLD model of the PI3K γ / LY294002 (1E7V model). The 1E7V active site contains charged residues Lys833, Asp841, Glu880, and Asp964 (Figure 2A). These charged residues suggest that the QPLD charge model based on

the protein environment would perform better than the RESP charge model, where partial charges are developed based on an isolated ligand. This prediction is consistent with what we have observed in our previous DNA/duocarmycin studies where DNA carries multiple charged phosphate groups.²⁰ This is exactly what we found with PI3K γ ; the contribution of electrostatic interactions was greater in the QPLD model (-21.9 kcal/mol) than that in the RESP (-6.8 kcal/mol). However, it is interesting to observe that during the MD simulations, the movement of charges residues resulted in a conformation at the fourth ns snapshot with only two charged residues retained: Glu880 and Asp964 in the QPLD model, and only Glu880 observed in the RESP charged model. Inspection of the electrostatic map of PI3K γ (1E7V) of these two charged models showed that the QPLD model contained a H-bond donor region (blue region surrounding Asp964, Figure 3B) because of the presence of Asp964, allowing electrostatic attraction with a H-bond acceptor of the carbonyl oxygen in LY294002. Such an interaction was absent in the RESP charge model (Figure 3).

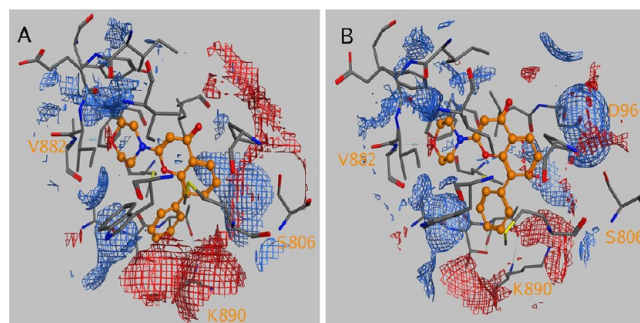


Figure 3. Electrostatic surface of the binding pockets of PI3K γ / LY294002: (A) RESP charged model and (B) QPLD charged model. Color code: H-bond receptor, red; and H-bond donor, blue. The electrostatic surfaces were made with the MOE program.

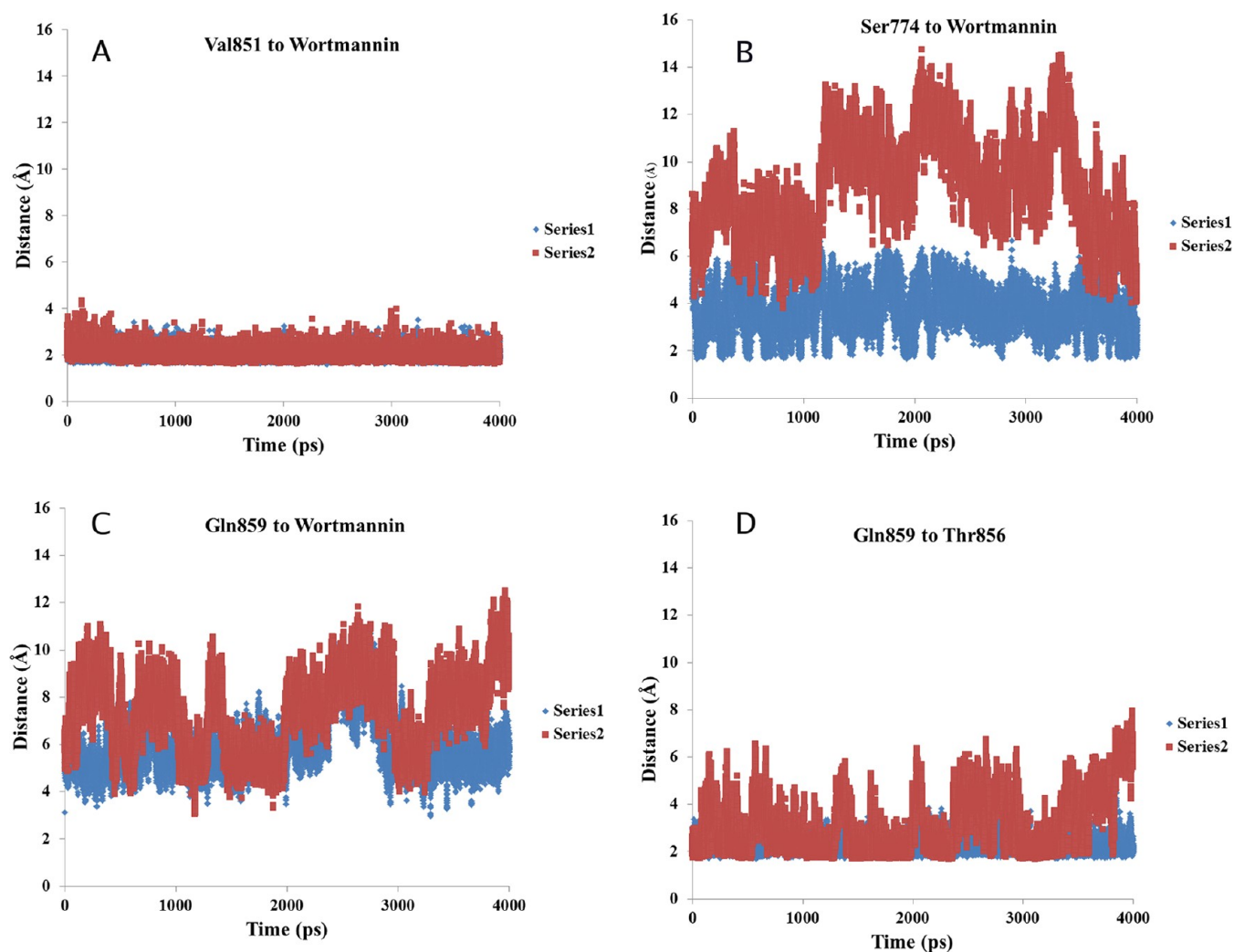


Figure 4. Distance proteins and ligands: (A) distance between Val851 NH of PI3K α and wortmannin O6 (RESP models), series 1 (blue, MUT model, 2.0 ± 0.2 Å), series 2 (red, wt model, 2.1 ± 0.2 Å); (B) distance between Ser773 OH of PI3K α and wortmannin O8 (RESP models), series 1 (blue, MUT model, 3.7 ± 0.9 Å), series 2 (red, wt model, 8.9 ± 2.1 Å); (C) distance between Gln859 NE2 of PI3K α and wortmannin O7 (RESP models), series 1 (blue, MUT model, 5.9 ± 1.1 Å), series 2 (red, wt model, 7.3 ± 1.6 Å); and (D) distance between Gln859 NH and Thr856 OG1 of PI3K α (QPLD models), series 1 (blue, MUT model, 2.2 ± 0.3 Å), series 2 (red, wt model, 3.1 ± 1.2 Å);

3.3. Mutant- or Isoform-Specific Binding. All six models have H-bond interactions between Val851 (PI3K α wt or MUT), or Val882 (PI3K γ) and ligand (wortmannin or LY294002). The distance between the Val851 backbone NH and the O6 of wortmannin was stabilized around 2.0 Å for both the wt and MUT PI3K α models (Figure 4A). This explains the lack of selectivity of many PIK inhibitors that were designed to target PI3K α Val851 (or Val882 in the γ -isoform). In the RESP model, the Ser774 in the PI3K α MUT forms a stable H-bond with a wortmannin oxygen with a distance of 3.7 ± 0.9 Å. The distance for the same pair of atoms in the WT PI3K α was 8.9 ± 2.1 Å. Therefore, our data suggests that Ser774 can be used to design mutant-specific inhibitors of PI3K α . Gln859 in the MUT model is closer to the wortmannin O7 (distance, 5.9 ± 1.1 Å) than that in the WT (distance, 7.3 ± 1.6 Å, Figure 4C). In the MUT (RESP model), the distance between Gln859 and wortmannin was around 4 Å for more than half of the simulations; in other words, the H-bonds between Gln859 and wortmannin were broken during at least half of the simulation time. This implies that Gln859 may not be as significant as Ser774 for mutant-specific ligand binding. Further investigation

of residue Gln859 showed that it played a significant role in maintaining the H-bond network of the binding pocket; the distance between the Gln859 backbone NH and the Thr856 side chain OH was stable at 2.2 ± 0.3 Å in the MUT model, whereas the same distance in the wt model was 3.1 ± 1.2 Å (Figure 4D). The favorable interactions of Ser774 and Gln859 for ligand binding to the H1047R mutant PI3K α were also observed in our previous docking studies.¹² Therefore, it is critical to take into account residues Ser774 and Gln859 for ligand design targeting H1047R MUT.

The electrostatic potential surface maps of the WT and MUT PI3K α proteins with the RESP and QPLD charge models provided further evidence of the role of Ser774 and Gln859 in mutant-specific ligand binding. The commonality between the four PI3K α models are Asp933 and Val851, two important residues discussed elsewhere.^{11,12} Ser774 was observed in all PI3K α models except for the WT models (Figure 5), in accord with the H-bond patterns shown in Figure 1. Similarly, Gln859 formed a stable H-bond with Thr856 of 3HHM, whereas Gln859 was not even observed in the active site of the WT QPLD model (2RD0). Another difference between the wt and

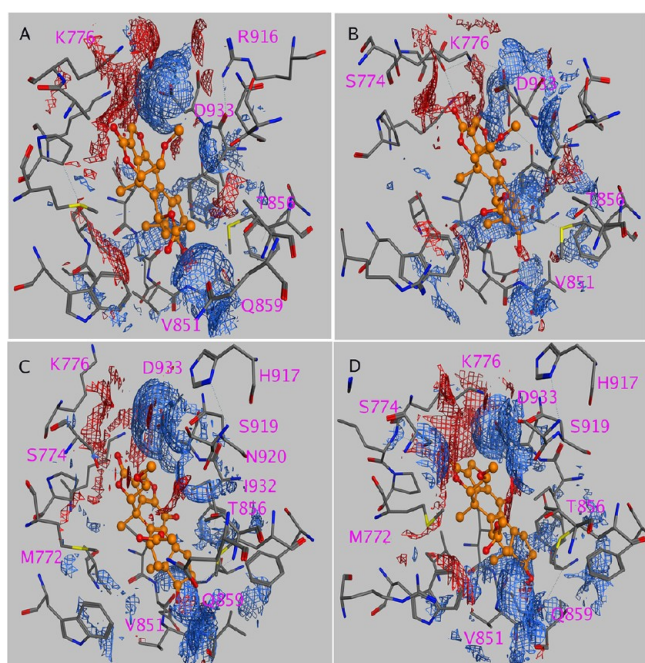


Figure 5. Electrostatic surface of the binding pockets of (A) wt PI3K α (RESP model); (B) wt PI3K α (QLPD model); (C) MUT PI3K α (RESP model); and (D) MUT PI3K α (QLPD model). Color code: H-bond receptor, red; and H-bond donor, blue. The electrostatic surfaces were made with the MOE program.

401 MUT PI3K α is the H-bond network in the binding pocket. In
 402 the MUT models, His917 forms H-bonds with Ser919, a polar
 403 residue that forms a dipole–dipole interaction with the
 404 carbonyl group of the wortmannin (Figure 5D). In the WT
 405 PI3K α model, Arg916 forms H-bonds with Asp933, another
 406 residue important for ligand binding. Neither Arg916 nor
 407 His917 were observed in the fourth ns snapshot of the WT
 408 QLPD model. The importance of designing H1047R mutant
 409 specific ligands would be the application to colon and breast
 410 cancer patients, among whom 30% carried H1047R mutation.
 411 This way, it would minimize the toxicity of inhibiting wild-type
 412 PI3K α . However, inhibiting wild-type PI3K α may be important
 413 for cancer types such as gastric cancer where overexpression of
 414 WT PI3K α is observed.

415 Sequence alignment between PI3K α and PI3K γ showed that
 416 Ser774, Val851, Gln859, and Asp933 of PI3K α correspond to
 417 residues Ser806, Val882, Lys890, and Asp964 of PI3K γ (for the
 418 whole sequence alignment, refer to reference 12 in the
 419 Supporting Information). An electrostatic potential surface
 420 shows that Gln859 in the PI3K α model is a H-bond donor
 421 (blue region, Figure 5) whereas Lys890 is a H-bond acceptor
 422 (red region, Figure 3). The position of Gln859 in PI3K α does
 423 play a role in ligand selectively binding to PI3Ks (the residues
 424 at this position is Lys890 in PI3K γ , and Asn836 in PI3K δ ^{42,43}).
 425 Figure 5 also shows that Lys776 is important for ligand binding
 426 to the α isoform since it provides a stabilizing H-bond
 427 interaction with Asp933. The corresponding residue in PI3K γ is
 428 Lys808, absent from the 4.5 Å interacting pocket. The
 429 ammonium group (NH₃⁺) of Lys890 adopts an extended
 430 conformation in the active site of PI3K γ (QLPD model),
 431 making it possible to serve as two H-bond acceptors (one from
 432 the side chain NH₃⁺, one from the main chain carbonyl
 433 oxygen). However, the same residue in the RESP model

pointed away from the binding site, allowing only one H-bond
 434 interaction with the backbone carbonyl group (Figure 3). 435

Therefore, although the overall RMSDs are similar between
 436 the RESP and QLPD charge models, individual residues,
 437 particularly those interacting with ligands, behave quite
 438 differently. The QLPD model, with improved prediction of
 439 electrostatic interactions, is able to reproduce the experimen-
 440 tally determined ΔG_{bind} . The overall free energies of binding in
 441 the H1047R mutant PI3K α model and in the γ model between
 442 RESP and QLPD charge systems are comparable and in accord
 443 with experimental values. 444

3.4. Hot Spot Residues at the Binding Interfaces

Unraveled by Computational Alanine Scanning. Hot spot
 446 residues in each interface were identified with the MM/GBSA
 447 method by mutating binding residues to alanine and comparing
 448 binding free energies of the mutants to that of the original
 449 protein. $\Delta\Delta G_{\text{bind}}$ is defined as ΔG_{bind} (alanine mutant) –
 450 ΔG_{bind} (wild-type). A positive $\Delta\Delta G_{\text{bind}}$ indicates an unfavorable
 451 mutation, that is, a ligand binds more favorably to the WT. In
 452 other words, a residue with a large positive $\Delta\Delta G_{\text{bind}}$ indicates
 453 that it is critical for ligand binding. On the other hand, a
 454 negative $\Delta\Delta G_{\text{bind}}$ indicates a preference for the alanine mutant,
 455 that is, a ligand binds more favorably to the mutant. The
 456 proline residue was not mutated because of its usual backbone
 457 conformation; replacing proline with alanine induces significant
 458 conformational changes and thus affects the binding mode.⁴⁴ 459

PIK3CA mutations can be used to predict resistance to two
 460 monoclonal antibodies (cetuximab and panitumumab) for
 461 suppressing epidermal growth factor receptor (EGFR) in
 462 metastatic colorectal cancer (mCRC) patients.⁴⁵ In patients
 463 with KRAS wild-type mCRC, a lower objective response rate
 464 was observed in patients with PIK3CA exon 20 mutations.⁴⁶ 465
 466 Among 377 patients, 62% carried WT KRAS and 38% with
 467 KRAS mutations. In both the KRAS WT and mutants group,
 468 89% of patients of mCRC have WT PIK3CA whereas 11%
 469 carried PIK3CA mutations.⁴⁶ A study of important binding
 470 residues in the WT and MUT PI3K α , therefore, is fundamental
 471 for mutant- or isoform-specific ligand design.

To determine the role of each binding residue in ligand
 472 binding to the wild-type or H1047R mutant of PI3K α , or
 473 PI3K γ , we systematically applied computational alanine
 474 scanning to active site binding residues (within 4.5 Å) of
 475 PI3Ks. The binding free energies ($\Delta\Delta G_{\text{subtot}}$) of WT PI3K α
 476 (QLPD charge model, Table 3) show that significant losses in
 477 the binding free energies were observed for the hydrophobic
 478 Val851, and Val850. In addition, the hydrophobic Trp780,
 479 Ile800, Tyr836, I848, Met922, and Ile932 showed $\Delta\Delta G_{\text{subtot}}$
 480 increase of greater than 2.5 kcal/mol. This indicates that a
 481 mutation of any of these residues would weaken ligand binding.
 482 Therefore, Trp780, Ile800, Tyr836, I848, Val850, Val851,
 483 Met922, and Ile932 can be called “resistant” mutants or “hot-
 484 spot” residues. This agrees with the energetic analysis of the
 485 binding free energy where van der Waals interactions are
 486 dominant. The prediction of Ile848 being an important binding
 487 residue ($\Delta\Delta G_{\text{subtot}}$ of 4.1) was corroborated by experimental
 488 observations that the mutant I848A possesses severely impaired
 489 enzyme activity (>100 fold weaker than the WT PI3K α).¹⁴ 490
 491 These data shows that these residues are significant for ligand/
 492 protein interactions.

Inspection of individual energy components (Table 3) of
 493 these mutations in the QLPD model shows that losses in
 494 hydrophobic interactions ($\Delta\Delta E_{\text{vdw}}$) contribute the most to the
 495 $\Delta\Delta G_{\text{subtot}}$ the relative energy of binding without the entropy 496

Table 3. Relative Free Energies of Binding (kcal/mol) for PI3K Alanine Mutants ($\Delta\Delta G_{\text{subtot}} = \Delta G_{\text{mutant}} - \Delta G_{\text{wt}}$) for the 2RD0 (WT QPLD model)^a

residues	$\Delta\Delta E_{\text{elec}}$	$\Delta\Delta E_{\text{vdw}}$	$\Delta\Delta G_{\text{SA}}$	$\Delta\Delta G_{\text{GB}}$	$\Delta\Delta G_{\text{solv}}$	$\Delta\Delta G_{\text{subtot}}$
M772	1.2	1.3	0.2	-1.2	-1.0	1.5
S774	0.4	0.7	0.1	-0.7	-0.6	0.5
K776	0.9	1.2	0.2	-1.3	-1.2	1.0
W780	5.0	4.0	0.6	-5.2	-4.6	4.5
I800	3.6	2.2	0.3	-3.3	-3.0	2.8
Y836	8.2	3.6	0.3	-8.2	-7.9	3.9
I848	3.6	3.6	0.4	-3.5	-3.1	4.1
E849	5.3	0.9	0.1	-4.9	-4.8	1.4
V850	1.4	0.8	0.0	7.7	7.7	9.9
V851	1.3	0.5	0.0	8.4	8.4	10.1
T856	-0.3	0.5	0.1	0.3	0.4	0.5
Q859	4.0	1.3	0.2	-4.3	-4.1	1.2
H917	0.4	0.0	0.0	-0.1	-0.1	0.4
M922	2.1	2.3	0.3	-1.8	-1.5	2.8
I932	3.2	4.5	0.3	-3.3	-3.0	4.7
D933	-0.8	1.6	0.1	0.7	0.8	1.5
D933/F934	-1.4	1.8	0.1	1.2	1.3	1.7
E970	1.5	0.0	0.0	-1.1	-1.1	0.4

^aThe energy components and standard deviations are listed in Supporting Information Table 3S.

497 component. One assumption of computational alanine
 498 scanning is that replacing the original residues with an alanine
 499 will cause only small local changes that have little effect on
 500 entropy, that is, the entropic terms ($-T\Delta S$) for the wild-type
 501 and the mutants should cancel out. The predominant factor for
 502 V850A and V851A is solvation energy loss ($\Delta\Delta G_{\text{solv}}$). For polar
 503 residues Tyr836, Glu849, Gln859, Met922, and Glu970,
 504 mutations to alanine lead to loss of electrostatic interactions
 505 (positive $\Delta\Delta E_{\text{elec}}$). A comparison of wild-type (2RD0) with
 506 H1047R mutant (3HHM) under the same QPLD model shows
 507 that Val850 and Val851 are important for ligand binding and
 508 thus highly unfavorable for mutating these two valines to
 509 alanines (Figure 6A), whereas the role of these two residues
 510 diminishes in the ligand binding toward H1047R mutant
 511 (Figure 6B).

To identify residues responsible for mutant-specific binding,
 we applied the same MM/GBSA method to binding residues in
 MUT H1047R PI3K α (Table 4). Compared to the WT PI3K α ,
 these mutations should be considered as double mutations.
 Data in Table 4 and Figure 6B show that in the MUT PI3K α
 model, Ile932, Trp780, Tyr836, and Met922 are residues
 critical for ligand binding to the MUT isoform. Similar to the
 WT model, losses in $\Delta\Delta E_{\text{vdw}}$ predominate for Trp780, Tyr836,
 and Met922. Although Ser774 $\Delta\Delta E_{\text{subtot}}$ in both the WT and
 MUT is less than 1 kcal/mol, the individual $\Delta\Delta E_{\text{elec}}$ energy
 components of 0.4 and 8.6 kcal/mol for the WT and MUT
 isoforms are quite different. As shown in Figure 4B, this may
 correspond to the loss of H-bonds in the MUT models.

The main difference between the WT and MUT hot spot
 residues lies in Val850, Val851, and Ile932. Val850 and Val851
 were predicted to be important in the WT (QPLD models),
 whereas Ile932 was predicted to be more critical in the H1047R
 mutant. In the MUT model, the $\Delta\Delta E_{\text{subtot}}$ of Ile932 was
 predicted to be 3.8 kcal/mol in the RESP model, and 14.6 kcal/
 mol in the QPLD model. In the RESP charge model, Val851
 and Ile932 would have almost identical $\Delta\Delta E_{\text{subtot}}$ values,
 indicating no mutant-specific binding implications. Under the
 QPLD charge model, Val851 appears to be more WT-specific
 and Ile932 more MUT-specific. Val850, on the other hand,
 shows importance to WT, but not to MUT ligand binding in
 both charge models. An inspection of the Ile932 interaction
 network shows that the Ile932 backbone NH in the QPLD
 MUT model formed a H-bond with side chain amide group of
 Asn920, stabilizing the binding pocket of MUT model (Figure
 5C). Similar to Ser774, the increase in $\Delta\Delta E_{\text{elec}}$ may be
 attributed to the loss of a H-bond stabilizing effect. Excluding
 Ile932, the correlation (R^2) of the $\Delta\Delta E_{\text{subtot}}$ between the
 QPLD and RESP models is 0.65 (Supporting Information
 Figure 2SA), suggesting both charge models would be able to
 predict the mutational effect of PI3K α .

To validate the MM/GBSA calculations in the MUT model,
 we performed double-mutations on the WT PI3K α , and
 compared the $\Delta\Delta G_{\text{subtot}}$ of these mutants to those of the
 H1047R MUT model. Our data showed that these two set of
 data yield a similar trend (Table 5). The linear relationship of
 the $\Delta\Delta G_{\text{subtot}}$ between these two models (R^2 of 0.69,

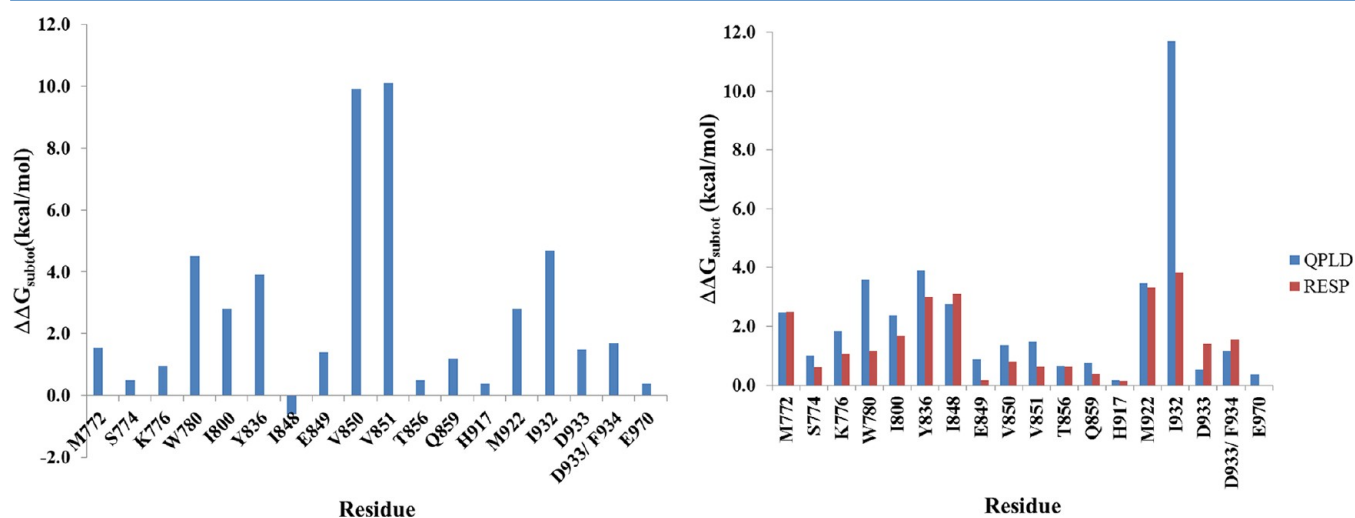


Figure 6. MM/GBSA binding free energy for (A) WT PI3K α (2RD0, QPLD model) and (B) H1047R MUT PI3K α (3HHM, both QPLD and RESP models).

Table 4. Relative Binding Free Energies (kcal/mol) for PI3K Alanine Mutants ($\Delta\Delta G_{\text{subtot}} = \Delta G_{\text{mutant}} - \Delta G_{\text{wt}}$) for the 3HHM MUT models (QPLD model)^a

residues	$\Delta\Delta E_{\text{elec}}$	$\Delta\Delta E_{\text{vdw}}$	$\Delta\Delta G_{\text{SA}}$	$\Delta\Delta G_{\text{GB}}$	$\Delta\Delta G_{\text{solv}}$	$\Delta\Delta G_{\text{subtot}}$	
						QPLD	RESP
M772	3.3	2.3	0.4	-3.6	-3.2	2.5	2.5
S774	8.6	-1.0	0.0	-6.6	-6.6	1.0	0.6
K776	-2.8	0.9	0.1	3.7	3.7	1.8	1.1
W780	0.2	2.8	0.3	0.2	0.6	3.6	1.2
I800	0.6	1.9	0.2	-0.4	-0.1	2.4	1.7
Y836	1.7	2.8	0.2	-0.8	-0.6	3.9	3.0
I848	-0.5	2.1	0.2	0.9	1.1	2.8	3.1
E849	3.0	0.1	0.0	-2.2	-2.2	0.9	0.2
V850	-0.7	0.8	0.0	1.2	1.3	1.4	0.8
V851	-0.7	0.6	0.0	1.6	1.6	1.5	0.6
T856	-0.5	0.5	0.1	0.5	0.6	0.6	0.6
Q859	-1.2	0.3	0.0	1.6	1.7	0.8	0.4
H917	0.4	0.2	0.0	-0.4	-0.4	0.2	0.1
M922	0.7	2.2	0.3	0.3	0.6	3.5	3.3
I932	-6.6	3.3	0.2	14.9	15.1	11.7	3.8
D933	-1.5	1.1	0.2	0.8	1.0	0.5	1.4
D933/F934	-0.8	1.6	0.2	0.2	0.3	1.2	1.6
E970	1.5	0.0	0.0	-1.1	-1.1	0.4	0.0

^aThe energy components and standard deviations are listed in Supporting Information Tables S5–S7S.

Table 5. Relative Free Energies of Binding (kcal/mol) for Double Mutants (Alanine Mutants of PI3K α Binding Residue Plus H1047R MUT, QPLD Model)^a

residues	$\Delta\Delta E_{\text{elec}}$	$\Delta\Delta E_{\text{vdw}}$	$\Delta\Delta G_{\text{SA}}$	$\Delta\Delta G_{\text{GB}}$	$\Delta\Delta G_{\text{solv}}$	$\Delta\Delta G_{\text{subtot}}$	
						QPLD (double mutant)	QPLD (3HHM)
E849 + H1047	3.6	0.1	0.0	-3.1	-3.1	0.6	0.9
D933 + H1047	-1.4	1.6	0.1	1.2	1.3	1.4	0.5
I848 + H1047	2.5	2.8	0.3	-2.0	-1.7	3.5	2.8
I800 + H1047	1.4	1.4	0.2	-1.0	-0.8	1.9	2.4
Y836 + H1047	5.0	3.0	0.2	-5.2	-5.0	2.9	3.9
W780 + H1047	2.3	3.0	0.4	-2.5	-2.1	3.2	3.6
V851 + H1047	1.1	0.5	0.0	-1.1	-1.1	0.5	1.5
V850 + H1047	1.6	0.8	0.0	-1.7	-1.7	0.7	1.4

^aThe $\Delta\Delta G_{\text{subtot}}$ values from the QPLD (3HHM model, Table 4) are listed for comparison. The energy components and standard deviations are listed in Supporting Information Table S8S.

Supporting Information Figure 2SB) further verified the reliability of using computational alanine scanning to predict the residue behaviors because of alanine mutation. The validation of double mutational effects can also be illustrated in the D933A/F934A mutant: the $\Delta\Delta G_{\text{subtot}}$ for this double mutant in the WT QPLD model is 1.7 kcal/mol (Table 3), suggesting an adverse effect of this double mutant, consistent with a complete loss of enzymatic activity of the double mutant D933A/F934A.¹³ Zunder et al.¹⁵ observed that mutants I800L, I800M, and I848V required 10-fold or higher concentrations to reach the enzymatic activity of the H1047R mutant, indicating that mutations on residues I800 and I848 of MUT H1047R are not favorable. Our calculations of I800A and V848A in the MUT model (2.4 and 2.8 kcal/mol, respectively, Table 4) and in the double mutant WT model (1.9 and 3.5 kcal/mol, respectively, Table 5) further confirm the unfavorable mutation of these two residues. These two residues, however, may not be mutant-specific in that the I800A and V848A in the WT models show QPLD model $\Delta\Delta G_{\text{subtot}}$ of 2.8 and 4.1 kcal/mol, respectively. Therefore, MM/GBSA alanine scanning suggests that Ile932 and Ser774 might be mutant-specific.

To identify residues responsible for isoform-specific binding, we applied computational alanine scanning to PI3K γ residues Ser806, Trp812, Ile831, Tyr867, Ile879, Ile881, Val882, Thr886, Lys890, and Asp964, corresponding to PI3K α residues Ser774, Trp780, Ile800, Tyr836, Ile848, Val850, Val851, His855, Gln859, and Asp933, respectively. Figure 7 suggests that Ile831, Ile879, Trp812, and Lys890 are residues critical for ligand binding to PI3K γ . For PI3K γ , the QPLD charge model generally yielded a better $\Delta\Delta G_{\text{subtot}}$ than the RESP charge model. However, both charge models showed similar trends with a correlation of 0.73 (R^2 , Figure 7B). As Trp812, Ile831, and Ile879 of PI3K γ provide important hydrophobic interactions for ligand binding, so do Trp780, Ile800, and I848 for PI3K α . Therefore, these three residues may not be isoform-specific.

Alanine scanning of residues in PI3K γ showed that the QPLD model predicted four residues (Trp812, Ile831, Ile879, and Lys890) to be important for ligand binding, whereas the RESP charge model predicted only two (Trp812 and Ile831). Data in Figures 2 and 3 confirmed the importance of Lys890. According to the QPLD charge model, Lys890 of PI3K γ is predicted to be important for ligand binding ($\Delta\Delta G_{\text{subtot}}$ of 3.5

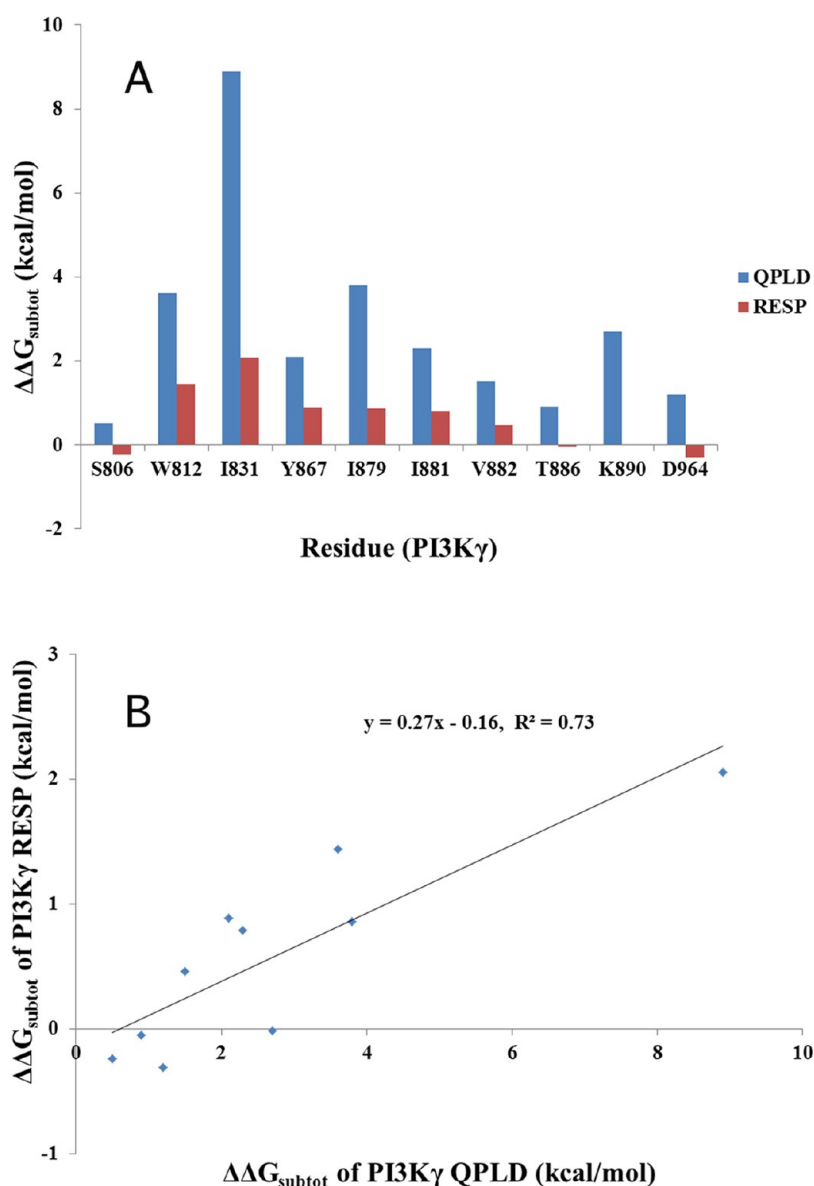


Figure 7. MM/GBSA binding free energy for PI3K γ (A), and the correlation between the QPLD and RESP charge models for PI3K γ (B). The energy components and standard deviations of 1E7 V/LY294002 interactions are listed in Supporting Information Tables 9S and 10S.

596 kcal/mol, Supporting Information Table 9S). Data in Figure 3
 597 shows that Lys890 in the QPLD-generated MD trajectory had
 598 two H-bond acceptor regions, while it only had one in the
 599 RESP charge model (which had a $\Delta\Delta G_{\text{subtot}}$ of 0 kcal/mol,
 600 Supporting Information Table 10S). According to site-directed
 601 mutagenesis,⁴⁷ Lys890 is a residue proved to be important for
 602 ligand's binding to PI3K γ . The amino group of Lys890 is
 603 oriented toward the binding cleft and therefore can form a
 604 stronger electrostatic interaction with wortmannin. In addition,
 605 the Lys890 main chain NH forms a H-bond with side chain
 606 hydroxyl group of Thr886 (Figure 8B). The corresponding
 607 residue in the α isoform is Gln859, which might be important
 608 for mutant-selective binding due to forming H-bonds with
 609 Thr856 (Figure 4D). For the WT PI3K α , such a H-bond is not
 610 stable due to its distance from the active site (not within the 4.5
 611 Å of bound ligand, Figures 5B, and 8A), Gln859 may not be
 612 critical for ligand binding to the α isoform and yet the
 613 corresponding residue in PI3K γ (Lys890) is important for
 614 binding. Therefore, Lys890 may be isoform-specific.

4. CONCLUSIONS

We applied molecular dynamics (MD) simulations to the WT 615
 and MUT PI3K α and PI3K γ based on RESP (restrained 616
 electrostatic potential) and quantum mechanics (QM)- 617
 polarized ligand docking (QPLD)-derived partial charges. 618
 The PI3K QPLD and RESP charge models show similar 619
 performance in MD simulations in terms of maintaining the 620
 stability of the aqueous systems. However, individual residues 621
 do behave differently, particularly for residues critical for 622
 mutant- or isoform-specific binding. We applied the GBSA 623
 method to estimate the binding free energies of wortmannin to 624
 PI3K α and, LY294002 to PI3K γ . The binding free energies of 625
 LY294002 to PI3K γ models (−9.3 and −9.5 kcal/mol) are in a 626
 very good agreement with the experiment (−9.2 kcal/mol), and 627
 the binding free energies of wortmannin to PI3K α models 628
 (−11.7 and −10.9) also agree with observed data (−10.9 kcal/ 629
 mol). MM/GBSA calculations suggested that residues Ser774, 630
 Gln859, and Ile932 might be used to design PI3K α mutant- 631

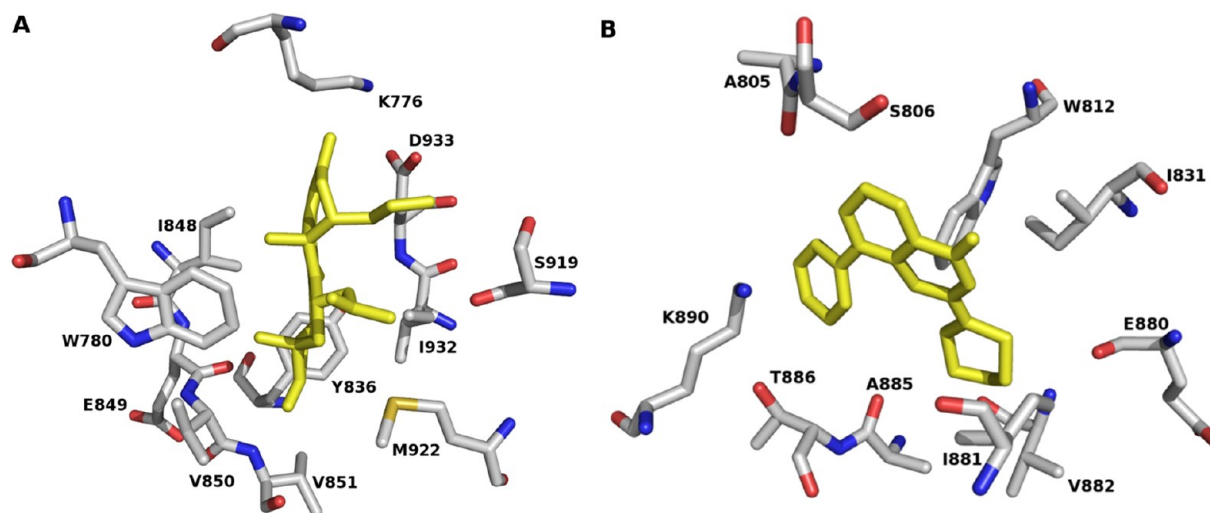


Figure 8. Binding pockets of (A) 2RD0 and (B) 1E7V. Ligands are represented in yellow color. Hydrogen atoms are hidden for clarity purpose.

632 specific ligands, whereas Lys890 can be used for PI3K γ ligand
633 design.

634 ■ ASSOCIATED CONTENT

635 ● Supporting Information

636 Atom types and atomic partial charges of wortmannin and
637 LY294002 and binding free energy components along with
638 standard deviations for MD simulation models. This material is
639 available free of charge via the Internet at <http://pubs.acs.org>.

640 ■ AUTHOR INFORMATION

641 Corresponding Author

642 *Tel. +1 402 554 3145. Fax: +1 402 554-3888. E-mail:
643 hzhong@unomaha.edu.

644 Present Address

645 Current address for Dima A. Sabbah: College of Pharmacy, Al-
646 Zaytoonah Private University of Jordan, P.O. Box 130, Amman
647 11733, Jordan.

648 Notes

649 The authors declare no competing financial interest.

650 ■ ACKNOWLEDGMENTS

651 This work was partially supported by the Research Corporation
652 for Science Advancement. DAS acknowledges Al-Zaytoonah
653 Private University of Jordan for financial support, and a Bukey
654 Fellowship from the University of Nebraska Medical Center.

655 ■ REFERENCES

656 (1) Vivanco, I.; Sawyers, C. L. The phosphatidylinositol 3-kinase-
657 AKT pathway in human cancer. *Nat. Rev. Cancer* **2002**, *2*, 489–501.
658 (2) Sabbah, D. A.; Brattain, M. G.; Zhong, H. Dual inhibitors of
659 PI3K/mTOR or mTOR-selective inhibitors: Which way shall we go?
660 *Curr. Med. Chem.* **2011**, *18*, 5528–5544.
661 (3) Rueckle, T.; Schwarz, M. K.; Rommel, C. PI3K gamma
662 inhibition: Towards an “aspirin of the 21st century”. *Nat. Rev. Drug*
663 *Discovery* **2006**, *5*, 903–918.
664 (4) Samuels, Y.; Wang, Z.; Bardelli, A.; Silliman, N.; Ptak, J.; Szabo,
665 S.; Yan, H.; Gazdar, A.; Powell, D.; Riggins, G.; Willson, J.; Markowitz,
666 S.; Kinzler, K.; Vogelstein, B.; Velculescu, V. High frequency of
667 mutations of the PIK3CA gene in human cancers. *Science* **2004**, *304*,
668 554–554.

(5) Liu, P.; Cheng, H.; Roberts, T. M.; Zhao, J. J. Targeting the
669 phosphoinositide 3-kinase pathway in cancer. *Nat. Rev. Drug Discovery*
670 **2009**, *8*, 627–644.

(6) Mandelker, D.; Gabelli, S.; Schmidt-kittler, O.; Zhu, J.; Cheong,
672 I.; Huang, C. H.; Kinzler, K.; Vogelstein, B.; Amzel, M. A frequent
673 kinase domain mutation that changes the interaction between PI3KR
674 and the membrane. *Proc. Natl. Acad. Sci. U. S. A.* **2009**, *106*, 16996–
675 17001.

(7) Kang, S. Y.; Bader, A. G.; Vogt, P. K. Phosphatidylinositol 3-
677 kinase mutations identified in human cancer are oncogenic. *Proc. Natl.*
678 *Acad. Sci. U. S. A.* **2005**, *102*, 802–807.

(8) Liu, Z. N.; Roberts, T. M. Human tumor mutants in the p110
680 alpha subunit of PI3K. *Cell Cycle* **2006**, *5*, 675–677.

(9) Shi, J.; Yao, D.; Liu, W.; Wang, N.; Lu, H.; Zhang, G.; Ji, M.; Xu,
682 L.; He, N.; Shi, B.; Hou, P. Highly frequent PIK3CA amplification is
683 associated with poor prognosis in gastric cancer. *BMC Cancer* **2012**,
684 *12*, No. 50.

(10) Vermaat, J. S.; Nijman, I. J.; Koudijs, M. J.; Gerritse, F. L.;
686 Scherer, S. J.; Mokry, M.; Roessingh, W. M.; Lansu, N.; De Bruijn, E.;
687 Van Hillegersberg, R.; Van Diest, P. J.; Cuppen, E.; Voest, E. E.
688 Primary colorectal cancers and their subsequent hepatic metastases are
689 genetically different: Implications for selection of patients for targeted
690 treatment. *Clin. Cancer Res.* **2012**, *18*, 688–699.

(11) Han, M.; Zhang, J. Z. H.; Class, I. Phospho-inositide-3-kinases
692 (PI3Ks) isoform-specific inhibition study by the combination of
693 docking and molecular dynamics simulation. *J. Chem. Inf. Model.* **2010**,
694 *50*, 136–145.

(12) Sabbah, D. A.; Vennerstrom, J. L.; Zhong, H. Docking studies
696 on isoform-specific inhibition of phosphoinositide-3-kinases. *J. Chem.*
697 *Inf. Model.* **2010**, *50*, 1887–1898.

(13) Stirdivant, S. M.; Ahern, J.; Conroy, R. R.; Barnett, S. F.; Ledder,
699 L. M.; Oliff, A.; Heimbros, D. C. Cloning and mutagenesis of the
700 p110 alpha subunit of human phosphoinositide 3'-hydroxykinase.
701 *Bioorg. Med. Chem.* **1997**, *5*, 65–74.

(14) Alaimo, P. J.; Knight, Z. A.; Shokat, K. M. Targeting the
703 gatekeeper residue in phosphoinositide 3-kinases. *Bioorg. Med. Chem.*
704 **2005**, *13*, 2825–2836.

(15) Zunder, E. R.; Knight, Z. A.; Houseman, B. T.; Apsel, B.;
706 Shokat, K. M. Discovery of drug-resistant and drug-sensitizing
707 mutations in the oncogenic PI3K isoform p110 α . *Cancer Cell* **2008**,
708 *14*, 180–192.

(16) Huang, C.; Mandelker, D.; Schmidt-Kittler, O.; Samuels, Y.;
710 Velculescu, V. E.; Kinzler, K. W.; Vogelstein, B.; Gabelli, S. B.; Amzel,
711 L. M. The structure of a human p110 alpha/p85 alpha complex
712 elucidates the effects of oncogenic PI3K alpha mutations. *Science* **2007**,
713 *318*, 1744–1748.

- 715 (17) Massova, I.; Kollman, P. A. Computational alanine scanning to
716 probe protein-protein interactions: A novel approach to evaluate
717 binding free energies. *J. Am. Chem. Soc.* **1999**, *121*, 8133–8143.
- 718 (18) Zhong, H. Z.; Carlson, H. A. Computational studies and
719 peptidomimetic design for the human p53-MDM2 complex. *Proteins:
720 Struct., Funct., Bioinf.* **2005**, *58*, 222–234.
- 721 (19) Cho, A. E.; Guallar, V.; Berne, B. J.; Friesner, R. Importance of
722 accurate charges in molecular docking: Quantum mechanical/
723 molecular mechanical (QM/MM) approach. *J. Comput. Chem.* **2005**,
724 *26*, 915–931.
- 725 (20) Zhong, H.; Kirschner, K. N.; Lee, M.; Bowen, J. P. Binding free
726 energy calculation for duocarmycin/DNA complex based on the
727 QPLD-derived partial charge model. *Bioorg. Med. Chem. Lett.* **2008**, *18*,
728 542–545.
- 729 (21) Walker, E. H.; Pacold, M. E.; Perisic, O.; Stephens, L.; Hawkins,
730 P. T.; Wymann, M. P.; Williams, R. L. Structural determinants of
731 phosphoinositide 3-kinase inhibition by wortmannin, LY294002,
732 quercetin, myricetin, and staurosporine. *Mol. Cell* **2000**, *6*, 909–919.
- 733 (22) *The Molecular Operating Environment (MOE)*; Chemical
734 Computing Group Inc.; Montreal, Quebec, Canada, 2009.
- 735 (23) Frisch, M. J.; Trucks, G. W.; Schlegel, H. B.; Scuseria, G. E.;
736 Robb, M. A.; Cheeseman, J. R.; Montgomery, J., J. A.; Vreven, T.;
737 Kudin, K. N.; Burant, J. C.; Millam, J. M.; Iyengar, S. S.; Tomasi, J.;
738 Barone, V.; Mennucci, B.; Cossi, M.; Scalmani, G.; Rega, N.;
739 Petersson, G. A.; Nakatsuji, H.; Hada, M.; Ehara, M.; Toyota, K.;
740 Fukuda, R.; Hasegawa, J.; Ishida, M.; Nakajima, T.; Honda, Y.; Kitao,
741 O.; Nakai, H.; Klene, M.; Li, X.; Knox, J. E.; Hratchian, H. P.; Cross, J.
742 B.; Bakken, V.; Adamo, C.; Jaramillo, J.; Gomperts, R.; Stratmann, R.
743 E.; Yazyev, O.; Austin, A. J.; Cammi, R.; Pomelli, C.; Ochterski, J. W.;
744 Ayala, P. Y.; Morokuma, K.; Voth, G. A.; Salvador, P.; Dannenberg, J.
745 J.; Zakrzewski, V. G.; Dapprich, S.; Daniels, A. D.; Strain, M. C.;
746 Farkas, O.; Malick, D. K.; Rabuck, A. D.; Raghavachari, K.; Foresman,
747 J. B.; Ortiz, J. V.; Cui, Q.; Baboul, A. G.; Clifford, S.; Cioslowski, J.;
748 Stefanov, B. B.; Liu, G.; Liashenko, A.; Piskorz, P.; Komaromi, I.;
749 Martin, R. L.; Fox, D. J.; Keith, T.; Al-Laham, M. A.; Peng, C. Y.;
750 Nanayakkara, A.; Challacombe, M.; Gill, P. M. W.; Johnson, B.; Chen,
751 W.; Wong, M. W.; Gonzalez, C. *Gaussian 03*, revision C.02; Gaussian,
752 Inc.: Wallingford, CT, 2004.
- 753 (24) Case, D. A.; Darden, D. A.; Cheatham, L. T. E.; Simmerling, C.
754 L.; Wang, J.; Duke, R. E.; Luo, R.; Crowley, M.; Walker, R. C.; Zhang,
755 W.; Merz, K. M.; Wang, B.; Hayik, S.; Roitberg, A.; Seabra, G.;
756 Kolossvary, I.; Wong, K. F.; Paesani, F.; Vanicek, J.; Wu, X.; Brozell, S.
757 R.; Steinbrecher, T.; Gohlke, H.; Yang, L.; Mongan, J.; Hornak, V.;
758 Kollman, P. A. *AMBER10*; University of California: San Francisco, CA,
759 2008.
- 760 (25) *Protein Preparation Wizard; Maestro; MacroModel; Phase, QM-
761 Based Ligand Docking; Glide*; Schrödinger, LLC: Portland, OR, 2009.
- 762 (26) Hornak, V.; Abel, R.; Okur, A.; Strockbine, B.; Roitberg, A.;
763 Simmerling, C. Comparison of multiple amber force fields and
764 development of improved protein backbone parameters. *Proteins:
765 Struct., Funct., Bioinf.* **2006**, *65*, 712–725.
- 766 (27) Jorgensen, W. L.; Chandrasekhar, J.; Madura, J. D.; Impey, R.
767 W.; Klein, M. L. Comparison of simple potential functions for
768 simulating liquid water. *J. Chem. Phys.* **1983**, *79*, 926–935.
- 769 (28) Darden, T.; York, D.; Pedersen, L. Particle mesh Ewald—An
770 $N\log(n)$ method for Ewald sums in large systems. *J. Chem. Phys.* **1993**,
771 *98*, 10089–10092.
- 772 (29) Tsui, V.; Case, D. A. Molecular dynamics simulations of nucleic
773 acids with a generalized Born solvation model. *J. Am. Chem. Soc.* **2000**,
774 *122*, 2489–2498.
- 775 (30) Bashford, D.; Case, D. A. Generalized Born models of
776 macromolecular solvation effects. *Annu. Rev. Phys. Chem.* **2000**, *51*,
777 129–152.
- 778 (31) Jayaram, B.; Sprous, D.; Beveridge, D. L. Solvation free energy
779 of biomacromolecules: Parameters for a modified generalized Born
780 model consistent with the AMBER force field. *J. Phys. Chem. B* **1998**,
781 *102*, 9571–9576.
- (32) Scanner, M. F.; Olson, A. J.; Spohner, J. C. Reduced surface: An
efficient way to compute molecular surfaces. *Biopolymers* **1996**, *38*,
305–320.
- (33) Case, D. A. Normal-mode analysis of protein dynamics. *Curr.
Opin. Struct. Biol.* **1994**, *4*, 285–290.
- (34) Kottalam, J.; Case, D. A. Langevin modes of macromolecules—
Applications to Crambin and DNA hexamers. *Biopolymers* **1990**, *29*,
1409–1421.
- (35) Perdih, A.; Bren, U.; Solmajer, T. Binding free energy
calculations of *N*-sulphonyl-glutamic acid inhibitors of MurD ligase.
J. Mol. Model. **2009**, *15*, 983–996.
- (36) Brown, K. L.; Bren, U.; Stone, M. P.; Guengerich, F. P. Inherent
stereospecificity in the reaction of aflatoxin B(1) 8,9-epoxide with
deoxyguanosine and efficiency of DNA catalysis. *Chem. Res. Toxicol.*
2009, *22*, 913–917.
- (37) Udommaneehanakit, T.; Rungrotmongkol, T.; Bren, U.; Freceer,
V.; Stanislav, M. Dynamic behavior of avian influenza A virus
neuraminidase subtype H5N1 in complex with oseltamivir, zanamivir,
peramivir, and their phosphonate analogues. *J. Chem. Inf. Model.* **2009**,
49, 2323–2332.
- (38) Bren, U.; Hodoscek, M.; Koller, J. Development and validation
of empirical force field parameters for netropsin. *J. Chem. Inf. Model.*
2005, *45*, 1546–1552.
- (39) Hon, W. C.; Berndt, A.; Williams, R. L. Regulation of lipid
binding underlies the activation mechanism of class IA PI3-kinases.
Oncogene **2012**, *31*, 3655–3666.
- (40) Bren, U.; Martinek, V.; Florián, J. Decomposition of the
solvation free energies of deoxyribonucleoside triphosphates using the
free energy perturbation method. *J. Phys. Chem. B* **2006**, *110*, 12782–
12788.
- (41) Bren, M.; Florián, J.; Mavri, J.; Bren, U. Do all pieces make a
whole? Thiele cumulants and the free energy decomposition. *Theor.*
Chem. Acc. **2007**, *117*, 535–540.
- (42) Murray, J. M.; Sweeney, Z. K.; Chan, B. K.; Balazs, M.; Bradley,
E.; Castanedo, G.; Chabot, C.; Chantry, D.; Flagella, M.; Goldstein, D.
M.; Kondru, R.; Lesnick, J.; Li, J.; Lucas, M. C.; Nonomiya, J.; Pang, J.;
Price, S.; Salphati, L.; Safina, B.; Savy, P. P.; Seward, E. M.; Ultsch, M.;
Sutherland, D. P. Potent and highly selective benzimidazole inhibitors of
PI3-kinase delta. *J. Med. Chem.* **2012**, *55*, 7686–7695.
- (43) Berndt, A.; Miller, S.; Williams, O.; Le, D. D.; Houseman, B. T.;
Pacold, J. I.; Gorrec, F.; Hon, W. C.; Liu, Y.; Rommel, C.; Gaillard, P.;
Rückle, T.; Schwarz, M. K.; Shokat, K. M.; Shaw, J. P.; Williams, R. L.
The p110 delta structure: mechanisms for selectivity and potency of
new PI(3)K inhibitors. *Nat. Chem. Biol.* **2010**, *6*, 117–124.
- (44) Clackson, T.; Ultsch, M. H.; Wells, J. A.; de Vos, A. M.
Structural and functional analysis of the 1:1 growth hormone/receptor
complex reveals the molecular basis for receptor affinity. *J. Mol. Biol.*
1998, *277*, 1111–1128.
- (45) Moroni, M.; Veronese, S.; Benvenuti, S.; Marrapese, G.; Sartore-
Bianchi, A.; Di Nicolantonio, F.; Gambacorta, M.; Siena, S.; Bardelli, A.
Gene copy number for epidermal growth factor receptor (EGFR) and
clinical response to antiEGFR treatment in colorectal cancer: a cohort
study. *Lancet Oncol.* **2005**, *6*, 279–286.
- (46) Mao, C.; Yang, Z. Y.; Hu, X. F.; Chen, Q.; Tang, J. L. PIK3CA
exon 20 mutations as a potential biomarker for resistance to anti-
EGFR monoclonal antibodies in KRAS wild-type metastatic colorectal
cancer: A systematic review and meta-analysis. *Ann. Oncol.* **2012**, *23*,
1518–1525.
- (47) Frazzetto, M.; Suphioglu, C.; Zhu, J.; Schmidt-Kittler, O.;
Jennings, I. G.; Cranmer, S. L.; Jackson, S. P.; Kinzler, K. W.;
Vogelstein, B.; Thompson, P. E. Dissecting isoform selectivity of PI3K
inhibitors: the role of non-conserved residues in the catalytic pocket.
Biochem. J. **2008**, *414*, 383–390.